Journal of Ceramic Processing Research. Vol. 18, No. 8, pp. 617~620 (2017)

J O U R N A L O F
Ceramic Processing Research

Optical properties of natural pyralspite garnets: The effect of electron beam irradiation

Sora Shin[a], Kyoung Deok Kim[a], Heeyul Park[b] and Jongwan Park[a]
[a]*Department of Materials Science and Engineering, Hanyang University 04763, Korea*
[b]*Department of Gem Dealers, Open Cyber University, 02087 Korea*

Almandine, pyrope and spessartine garnets were investigated. The samples were irradiated with 10 MeV electron energy to fluencies of 2×10^{17} cm^{-2} for one hour. After irradiation, the Cr^{3+} ion absorption band decreased but the Fe^{2+} ion increased in the UV-visible and Fourier transform infrared (FT-IR) spectra of pyrope garnets. In the spessartine samples, the absorption bands of Mn^{2+} decreased but Fe^{2+} increased. However, there was no significant change in the almandine garnet spectra. Electron paramagnetic resonance (EPR) was used to measure the changes in the electrovalence of the pyrope and spessartine garnets after irradiation. Pyrope garnets exhibited two peaks, a peak near g~1.98 attributed to Cr^{3+} in the octahedral position and a peak near g~2.01 attributed to Fe^{3+} in the octahedral position. Spessartine garnets had only one peak near g~2.04, attributed to Fe^{3+} in the octahedral position.

Key words: Electron beam, garnet, UV-Vis, FT-IR, EPR.

Introduction

Garnets, distinguished by their chemical composition, are designated as pyrope, almandine, spessartine (these three form the pyralspite subgroup), grossular, andradite, or uvarovite (these three form the ugrandite subgroup). Clear and transparent silicate minerals are known to have gemstone qualities. These minerals have been studied both mineralogically and gemologically [1]. Rhodolite is an iron-magnesium-aluminum silicate in the pyrope-almandine solid-solution series with an approximate garnet composition of $Py_{70}Al_{30}$. Garnets have chemical compositions of $A^{2+}{}_3B^{3+}{}_2(SiO_4)_3$, where A^{2+} is Fe^{2+}, Mg^{2+}, or Mn^{2+}, and B^{3+} is Al^{3+}. [2] The chemical composition of almandine is $Fe_3Al_2(SiO_4)_3$, pyrope is $Mg_3Al_2(SiO_4)_3$, spessartine is $Mn_3Al_2(SiO_4)_3$, and rhodolite is $(Mg, Fe)_3Al_2(SiO_4)_3$. As shown in Fig. 1, garnets consist of alternating SiO_4 tetrahedrals and BO_6 octahedrals that share corners to form a continuous, three-dimensional framework. The oxygen atoms in the framework also define a triangular dodecahedral consisting of eight oxygen atoms that coordinate with A cations. Each of these oxygen atoms coordinates with one Si, one B cation, and two A cations. As a result, there is a high percentage of shared edges [2].

Garnets are widely used gemstones. S. Utsunomiya and Adekeye irradiated garnets with ions and X-rays, respectively; however, electron beam irradiation of garnets has not been reported [3, 4]. Therefore, our work focused on investigating the electron beam irradiation process of garnets. After irradiation, the UV-visible, FT-IT, and EPR spectra were measured to confirm point defects in garnet crystals.

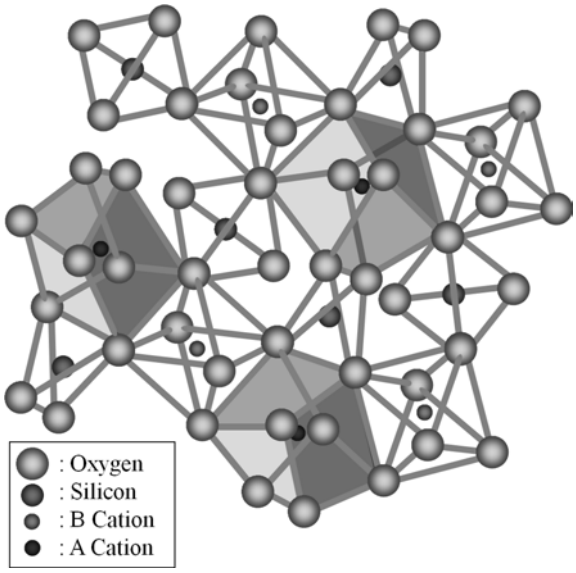

Fig. 1. The crystal structure of garnet is composed of Si and O ions. The B site contains Al^{3+}, Fe^{3+} or Cr^{3+}, and the A site contains Ca^{2+}, Mg^{2+} or Fe^{2+} [1].

Experimental Methods

For this study, faceted samples of untreated natural almandine (Al1, Al2, Al3), pryope (Py1, py2, py3), and spessartine (Sp1, Sp2, Sp3) garnet were examined in detail. The faceted samples were cleaned by immersion in

*Corresponding author:
Tel : +82-2-2220-0386
Fax: +82-2-2298-2850
E-mail: jwpark@hanyang.ac.kr

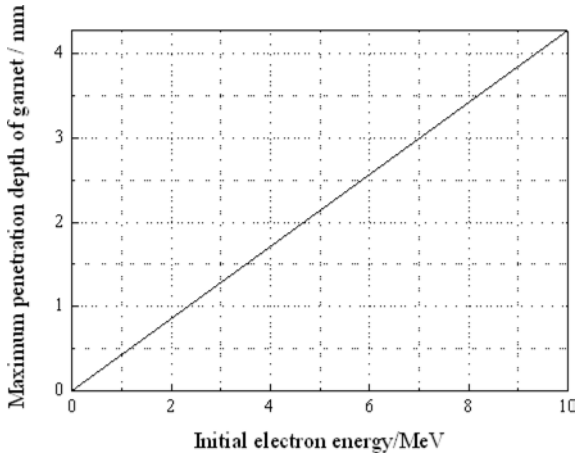

Fig. 2. Maximum penetration of electron damage in garnet versus electron energy.

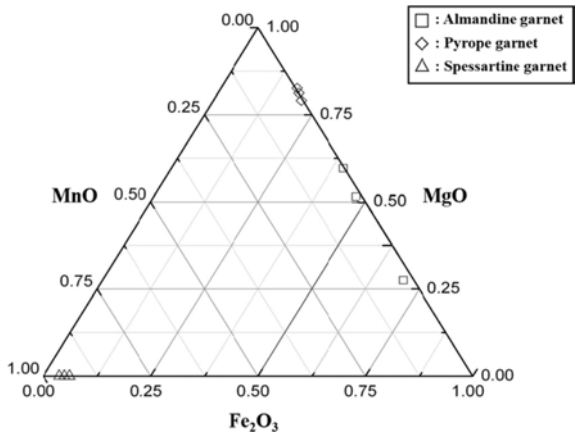

Fig. 3. Ternary diagram of the 9 garnet samples studied.

beaker distilled water and an ultrasonic bath for 10 min. The size of the samples ranged from $42 \times 41 \times 33$ to $85 \times 68 \times 26$ mm. The chemical compositions of samples were determined with X-ray fluorescence using a Shimadzu XRF-1700. The samples were irradiated in a 10 MeV electron accelerator to fluencies of 2×10^{17} cm^{-1} for 1 hr using a UELV-10-10s. Fig. 2 graphs the maximum penetration depth of the garnet based on a calculation defined by Brendan Campbell [5]. UV-Vis, mid-infrared and EPR spectra were taken before and after irradiation. UV-Vis spectroscopy analysis was performed from 300 to 800 nm using a JASCO V-650. Mid-infrared spectra were analyzed using a Jasco 4100 type FT-IR spectrometer in the range of 7000 to 3000 cm^{-1}. EPR spectra were observed from samples cut to less than 2 mm using a Jeol JES-FA200.

Results and Discussion

Table 1 reports the chemical compositions in terms of end-members. Al samples contained much more Fe than Mg, indicating they belong to the almandine-pyrope garnet group. Py samples had much more Mg than Fe, as in the pyrope-almandine garnet group. Sp samples were highly pure spessartine garnets. Fig. 3 shows a ternary diagram of the garnets according to

Table 1. Oxide components in garnet samples according to EDXRF analysis.

Sample no.	Almandine			Pyrope			Spessartine		
	Al 1	Al 2	Al 3	Py 1	Py 2	Py 3	Sp 1	Sp 2	Sp 3
Oxide (wt%)									
SiO_2	38.54	35.99	37.25	35.05	35.14	35.91	37.70	38.16	35.60
Al_2O_3	33.07	33.52	32.50	33.99	33.22	31.28	33.36	34.09	37.82
MgO	7.09	14.49	17.36	23.02	21.54	21.74	0.00	0.00	0.00
Fe_2O_3	17.92	13.47	11.98	5.23	5.07	5.56	0.85	1.11	1.29
CaO	2.26	1.80	0.37	3.77	3.34	3.98	0.23	0.25	0.21
MnO	0.71	0.34	0.12	0.24	0.19	0.15	26.77	25.60	23.88
Na_2O	0.19	0.15	0.23	0.33	0.27	0.22	0.64	0.43	0.64
CuO	nd	0.07	0.01	0.01	0.07	nd	0.03	nd	0.22
P_2O_5	0.15	0.05	0.08	0.03	0.03	0.02	0.21	0.15	0.19
K_2O	0.02	0.03	0.01	0.02	0.02	0.02	0.05	0.05	0.05
Cr_2O_3	0.05	0.03	0.06	1.08	1.01	1.03	0.03	0.04	nd
TiO_2	nd	0.02	0.03	0.12	0.06	0.06	nd	nd	nd
NiO	nd	nd	nd	nd	nd	nd	0.04	0.03	0.03
V_2O_5	nd	nd	nd	0.02	0.03	0.03	nd	nd	nd
OsO_4	nd	nd	nd	nd	nd	nd	nd	nd	nd
GeO_2	nd	nd	nd	nd	nd	nd	0.05	0.04	0.03
ZnO	nd	nd	nd	nd	nd	nd	0.05	0.04	0.02
Total	100.00	100.00	100.00	100.00	100.00	100.00	100.00	100.00	100.00

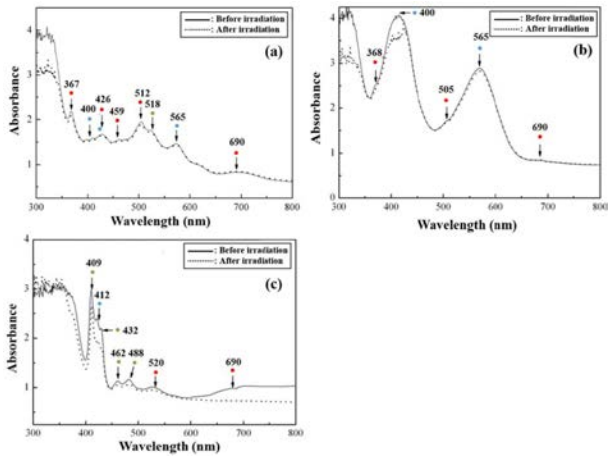

Fig. 4. UV-Vis absorption spectra (300-800 nm region) of various garnet samples before and after electron beam irradiation (red points: Fe^{3+}; blue points: Cr^{3+}; green points: Mn^{2+}): (a) Al sample, (b) py sample, and (c) sp sample.

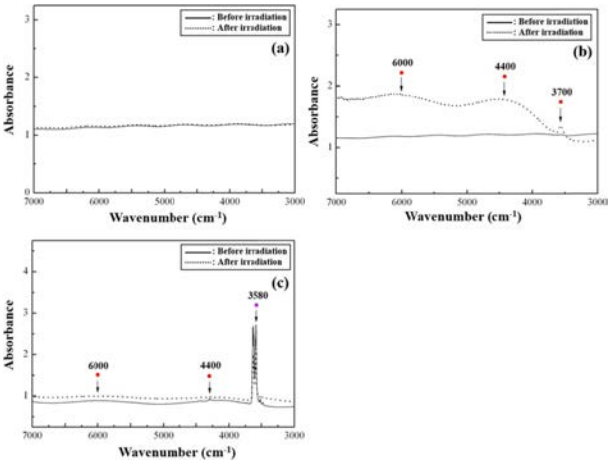

Fig. 5. Mid-infrared spectra (3000-7000 cm^{-1} region) of various garnet samples before and after electron beam irradiation (red point: Fe^{2+}, violet point: OH^{-}): (a) Al sample, (b) py sample, and (c) sp sample.

these data.

In garnets, the divalent metal ions are located predominantly in the distorted dodecahedral sites. Fe is the principal divalent cation in almandine as the spin-allowed 'd-d' transitions have absorption bands due to 8-coordinated, Fe(II). Based on the XRF data of pyrope, even if Fe(II) is not the principal divalent metal, considerable amounts of Fe(II) are often present. Spessartine garnets also contain Fe(II), with similar structures and different end-members in solid solution. Therefore, it is reasonable that all of the samples have similar peak positions [6].

Fig. 4 shows UV-Visible spectra of garnets before (solid line) and after (dotted line) electron beam irradiation. Al sample exhibited no significant changes, but notable changes were observed in the Py and Sp sample.

Fig. 4(a) illustrates the absorption peaks of Al sample. The $Fe^{3+}[^4T_2(^4G)$, $^4E_4A_1(^4G)]$ and $Cr^{3+}[^4T_2(^4F)$, $^4T_1(^4F)]$ in the octahedral positions were responsible for the absorption peaks at 367, 426, 459, 521, 690 nm and 400, 565 nm, respectively [6-9]. An absorption peak was observed at 518 nm for Mn^{2+} $[^4E^4A_1(^4G)$, $^4E(^4D)]$ in the dodecahedra position [10]. The absorption peaks of Py sample are illustrated in Fig. 4(b). After irradiation, Cr^{3+} and Fe^{3+} peaks decreased. The Fe^{3+} in the octahedral position contributed to absorption at 368, 505, and 690 nm. The absorption peaks at 400 and 565 nm are attributed to Cr^{3+} in the octahedral position [6-8].

Fig. 4(c) shows UV-Visible spectra of Sp sample. After irradiation, Mn^{2+} and Fe^{3+} peaks decreased. Absorption peaks due to Mn^{2+} were observed in the dodecahedral position at 409, 432, 462, and 488 nm. An absorption peak due to Cr^{3+} was observed in the octahedral position at 421 nm. Fe^{3+} was observed in the octahedral position at 690 nm. Sharp peaks at 409, 432, and 521 nm occurred due to the electronic transition of Mn^{2+} in the dodecahedral position [6-8].

Most crystals exhibited absorption bands in the range of 1000 to 3000 cm^{-1}. These spectra are associated with fundamental lattice absorption bands that are likely phonon overtone absorption regions of the SiO_4 band located at approximately 890 cm^{-1}. Two phonon overtones of SiO_4 were observed near 1760 cm^{-1} [7].

Fig. 5 shows the FT-IR spectra of the samples. There were significant changes in the Py and Sp samples however, there were no changes in the Al [Fig. 5(a)] sample. Fig. 5(b) shows FT-IR spectra of Py sample. After irradiation, the absorption band of the Py sample increased due to Fe^{2+} ($^5A_2(^5D)$, $^5A_4(^5D)$, $^5A_3(^5D)$) in the dodecahedral position at 6000, 4400 and 3700 cm^{-1} [7], [11]. Fig. 5(c) shows FT-IR spectra in the Sp sample. After irradiation, the peak at 3580 cm^{-1} decreased due to OH^{-}. The absorption bands at 3700, 4400 and 5600 cm^{-1} are attributed to the spin-allowed, crystal field transition of Fe^{2+} in the dodecahedral position [6, 7], [11, 12].

EPR spectra were measured in the Py and Sp samples. Py sample exhibited some spectral changes, as shown in Fig. 6(a). Two signals near g=1.98 and g = 2.01 were observed, and the lines were attributed to Cr^{3+} and Fe^{3+} ions in the octahedral positions [13, 14].

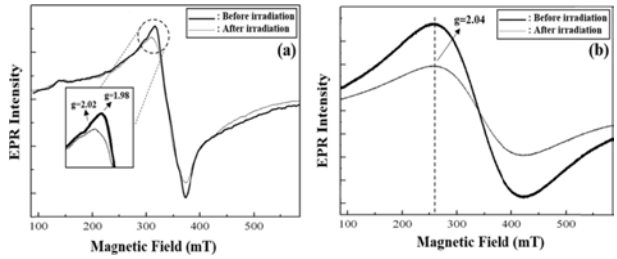

Fig. 6. EPR spectra of garnet samples before and after irradiation: (a) py sample, (b) sp sample.

After electron beam irradiation, UV-Visible, FT-IR, and EPR measurements of the samples showed some changes:

$$Cr^{3+} + Fe^{3+} \rightarrow Cr^{4+} + Fe^{2+} \quad (1)$$

Fig. 6(b) shows EPR spectra in the Sp sample. In the spectra, there was only one peak at g = 2.04, attributed to Fe^{3+} in an octahedral position [12, 15]. No peak related to Mn^{2+} was observed because the Fe^{3+} peak was too strong.

In the case of the Sp samples, we investigated UV-Visible, FT-IR spectra and EPR spectra by electron beam irradiation.

$$Mn^{2+} + 2Fe^{3+} \rightarrow Mn^{4+} + 2Fe^{2+} \quad (2)$$

Conclusions

The compositions of the nine samples were investigated through EDXRF analysis. The almandine garnets were dominated by Fe, pyrope garnets were dominated by Mg, spessartine samples were dominated by Mn.

The UV-Visible and FT-IR spectra were measured after irradiation. Many of the samples were changed by the electron beam irradiation. Cr^{3+} and Fe^{3+} peaks decreased and Fe^{2+} peaks increased in the pyrope garnets. In the case of the spessartine garnets, Mn^{2+} and Fe^{3+} peaks decreased and the Fe^{2+} peaks increased. EPR spectra were measured in the Pyrope and spessartine garnet. The pyrope garnets two main signals were observed near g = 1.98, designating Cr^{3+} in the octahedral position and g~2.01 for Fe^{3+} in the octahedral position. The pyrope garnets indicated Cr^{3+} was oxidized into Cr^{4+} in the octahedral position.

In the spessartine garnets, one broad peak near g~2.04 was observed for Fe^{3+} in the octahedral position. Alteration of the absorption bands, wavenumber, and EPR spectra after irradiation were attributed to the following reactions:

Pyrope garnet: $Cr^{3+} + Fe^{3+} + \text{e-beam} \rightarrow Cr^{4+} + Fe^{2+}$

Spessartine garnet: $Mn^{2+} + 2Fe^{3+} + \text{e-beam} \rightarrow Mn^{4+} + 2Fe^{2+}$.

However, almandine garnets did not exhibit significant change. Changes in the color and ionic valence of the garnets were observed by electron beam irradiation. However, the colors of the garnet samples did not show significant changes.

References

1. J.M. Yauri, N.F. Canoa, S. Watanabea, J. Lumin. 128[10] (2008) 1731-1737.
2. G.A. novak and G.V. Gibbs, Am. Mineral. 56 (1971) 791-825.
3. J.I.D Adekeye, N Y Sci. J. 2[4] (2009) 64-73.
4. S. Utsunomiya, L.M. Wang and R.C. Ewing, Nucl. Instr. Meth. Phys. Res. B. 191 (2002) 600-605.
5. B. Campbell, W. Choudhury, A. Mainwood, M. Newton and G. Davies, Nucl. Instr. Meth. Phys. Res. A 476[3] (2002) 680-685.
6. P.G. Manning, Can. Mineral. 9 (1967) 273-251.
7. G.A. Slack and R.M. Chrenko, et al., J. Opt. Soc. Am. 61[10] (1971). 1325-1329.
8. P.G. Manning, Can. Mineral. 11 (1972) 826-839.
9. K. Schmetzer and T. Hainschwang, J. Gemm. 38 (2002) 148-155.
10. P. G. Mamming, Can. Mineral. 10 (1970a) 677-681.
11. W.B. White and R.K. Moore, Am. Mineral. 57 (1972) 1692-1710.
12. J.C.R. Mittania and S. Watanabe, Radiat. J. Eff. Defect S. 159[8] (2004) 483-489.
13. W.B. Lewis, Appl. Phys. A. 54 (1992) 31-34.
14. G. Anbalagan, K. Sakthimurngesan, and M. Balakrishnan, Appl. Claya. Sci. 42[1], (2008) 175-179.
15. R.D. Dowsing and J.F. Gibson, Chem Phys. 50 (1969) 294-303.